Inchworm-like Robot Locomotion using Off-the-Shelf 3D-printable Anisotropic Friction Pads

Jiří Kubík, Anastázie Rišková, Jan Faigl
Faculty of Electrical Engineering, Czech Technical University in Prague, Czechia
{*kubikji2, riskoana, faiglj*}*@fel.cvut.cz*

1 Introduction

The herein-studied locomotion control is motivated by inchworm (Geometrid Moth caterpillar) movement coordinated in the looping gait where the limbs alternate between anchoring the inchworm to the surface and reaching a new anchoring point while moving forward. The anchoring has been replicated for inchworm robots using the flux-switching electromagnets for iCrawl [1] or suction cups for pipe inspection [2]. The addressed research question is to verify hypotheses on using the friction anisotropy observed in snakeskin to prevent the robot from sliding backward rather than deploying an explicit anchoring mechanism based on the assumption that it will enable efficient locomotion while reducing the overall complexity.

Figure 1: The designed robot resembles an inchworm with anisotropic friction pads formed by flexible scales for anchoring instead of the limbs found in its biological original.

Existing design approaches to mimic snake-skin-like materials include metallic 3D printed micro structures [3], sharp-bristled fabric [4], or soft silicon with embedded 3D printed structure and attached glass fiber resin scales [5]. Our approach uses flexible 3D printed macroscopic scales attached to contact segments of the proposed 4-DoF (*Degrees of Freedom*) hard 3D printed robot, depicted in Fig. 1. We report on experimental verification of the developed anisotropic friction pads in three types of inchworm-inspired gait. Although various methods from the literature report on replicated friction anisotropy, to the best of the authors' knowledge, using a single off-the-shelf 3D-printable flexible material is unique for inchworm robots.

2 Robot Design

The frictional anisotropy pads are 3D printed using the *Thermo-Plastic Elastomer* (TPE) FiberFlex 40D (Fiberlogy, Poland), with dimensions depicted in Fig. 2. When moving forward, the scales bend toward the robot's abdomen, while when moving backward, they interlock with the terrain, resisting motion and providing support as depicted in Fig. 1.

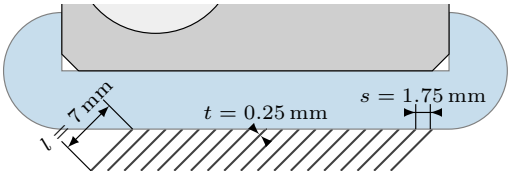

Figure 2: Developed scales xy-plane projection with length $l = 7$ mm, thickness $t = 0.25$ mm and spaced at $s = 1.75$ mm. In the z-axis, the scales are split into left, middle, and right rows in a 1:2:1 ratio.

The 4-DoF robot body depicted in Fig. 3 consists of four Dynamixel XM430-W350-R smart servomotors (Robotis, South Korea) and 3D printed brackets using *Polyethylene Terephthalate Glycol* (PETG) filament (Prusa Polymers, Czechia). The brackets enable $\pm 120°$ motion for the middle double bracket and $\pm 180°$ for the endpoint brackets from the prolonged position. At least 3 DoF are needed to control the robot prolongation while keeping the friction pads aligned with the terrain. The control of the friction pad's contact angle further exploits friction anisotropy, allowing the robot to switch contact materials and enhance friction differences between anchoring and moving segments. Since the friction depends on applied force, additional DoF enables load redistribution to increase anchoring efficiency.

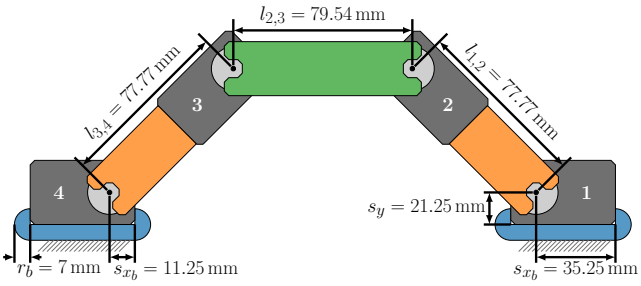

Figure 3: The kinematics parameters of the proposed robot that is composed of four servomotors (black), structural 3D printed links (orange and green) with respective minimum $\pm 120°$ and $\pm 180°$ rotation, anisotropic friction pads (grey), friction pad interfaces with cylindrical bumpers (blue).

3 Robot Control

The proposed robot is validated using the following three gait control methods. *Sliding gait* uses only the friction pad anisotropy to locomote in two-phase gait with *exten-*

sion and *contraction* as depicted in Fig. 4a. *Balancing gait* extends the sliding gait by moving *Center of Mass* (CoM) between the gait phases to increase (decrease) further the friction force for the anchoring pad (moving pad) as shown in Fig. 4b. *Stepping gait* extends the balancing gait by using the pad ends (bumpers) instead of the friction pad surface when moving the segment forward as outlined in Fig. 4c. Interpolation is used in between the key poses.

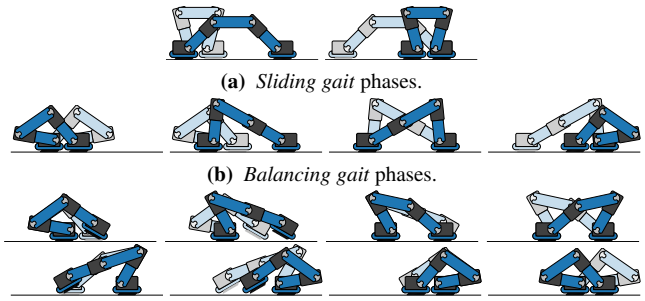

(a) *Sliding gait* phases.

(b) *Balancing gait* phases.

(c) *Stepping gait* phases.

Figure 4: Robot motion rigging in the hand-crafted locomotion gaits using anisotropic friction pads. The faded silhouette depicts the pose at the phase start, while the full color depicts the pose at the phase end.

4 Experimental Results

The proposed concept has been experimentally validated using three selected flat terrains: high-friction *Expanded Polyethylene* (EPE) with $\mu_f \approx 1.2$ forward and $\mu_b \approx 1.4$ backward friction coefficients, rough high-friction *Artificial Turf* (Grass) with $\mu_f \approx 0.75$, $\mu_b \approx 1.4$, and soft low-friction *Polyethylene Terephthalate Glycol* (PETG) with $\mu_f \approx 0.2$, $\mu_b \approx 0.2$, as shown in Fig. 5. Moreover, the 5° and 10° slopes are used for the EPE terrain.

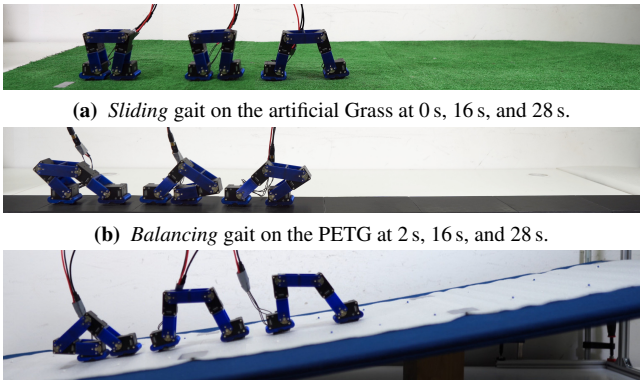

(a) *Sliding* gait on the artificial Grass at 0 s, 16 s, and 28 s.

(b) *Balancing* gait on the PETG at 2 s, 16 s, and 28 s.

(c) *Stepping* gait on 10°-sloped EPE at 3 s, 13 s, and 28 s.

Figure 5: Composed snapshots for selected terrains and gaits.

The developed gaits are deployed on flat and sloped terrains, and their performance is measured using the achieved average locomotion speed from ten trials lasting 30 s. The locomotion efficiency is examined using the expected locomotion speed under ideal conditions as the maximal robot prolongation and time spent expanding/contracting varies across the gaits. Furthermore, we explore the *Cost of Transport* (CoT) for each gait on each terrain using measured servomotor currents, known voltage $U = 12\,\mathrm{V}$, and the computed average robot speed. The performance indicators are depicted in Fig. 6.

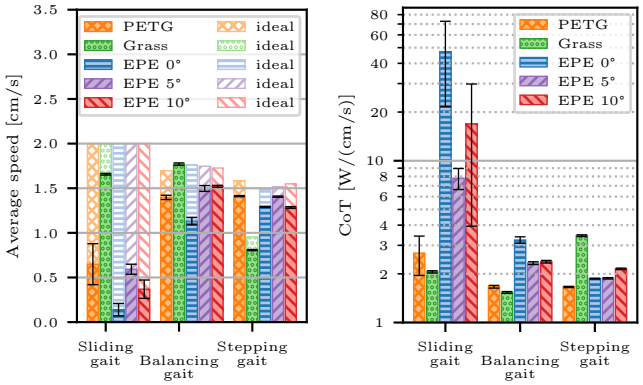

(a) Average locomotion speed **(b)** CoT

Figure 6: Locomotion performance in the selected scenarios. The expected speed under ideal conditions is depicted in light shade for each terrain and gait. CoT is depicted with the logarithmic scale on the y-axis.

The resulting plots in Fig. 6 suggest that all gaits are capable of locomoting the robot over the considered terrains. However, we observed that Sliding gait, which relies solely on the frictional anisotropy, struggles to anchor on smooth PETG and stick to EPE even when moving forward regardless of the terrain slope. Hence, it fails to reach the expected speed. Balancing and Stepping gaits consistently approach their potential regardless of the terrain. For sloped terrains, the front pad starts to slip backward slightly at the beginning of the retraction phase for all gaits. Although it stabilizes later within the same phase, it results in a notable average speed decrease. Managing CoM can significantly improve the locomotion performance to the extent that it is competitive with combining friction pads surface and bumpers.

5 Conclusion

The reported early results on the experimental validation of the proposed 3D-printable flexible scales-based anisotropic friction pads support the feasibility of the developed 3D-printed five-link inchworm-like robot using off-the-shelf materials and components. The robot's locomotion performance is evaluated using three gaits in five experimental setups using flat and sloped terrains. The results indicate that friction pads enable robot locomotion by assuming sufficient differences between forward and backward friction forces. The gaits that exploit a combination of two materials or managing CoM enable the robot to locomote in all examined scenarios. Since the presented results support the concept's viability, possible future work can be to extend the concept into full 3D locomotion by adding more DoF.

6 Acknowledgments

The authors express their gratitude to M. Škarytka and J. Bittner for their support during the testbed construction and to K. Kubíková for providing the real inchworm photography. The work has been supported by the Technology Agency of the Czech Republic under the project No. TN02000028. The support under grant No. SGS23/184/OHK3/3T/13 to the first author is also gratefully acknowledged.

References

[1] M. B. Khan, T. Chuthong, C. Danh Do, M. Thor, P. Billeschou, J. C. Larsen, and P. Manoonpong, "icrawl: An inchworm-inspired crawling robot," *IEEE Access*, vol. 8, pp. 200 655–200 668, 2020.

[2] Y. Zhou and Q. Zeng, "Inchworm robot structural design and kinematic modeling," in *International Conference on Computing, Robotics and System Sciences (ICRSS)*, 2022, pp. 1–5.

[3] C. Tiner, S. Bapat, S. D. Nath, S. V. Atre, and A. Malshe, "Exploring convergence of snake-skin-inspired texture designs and additive manufacturing for mechanical traction," *Procedia Manufacturing*, vol. 34, pp. 640–646, 2019.

[4] W. Saab, A. Kumar, and P. Ben-Tzvi, "Design and analysis of a miniature modular inchworm robot," in *International Design Engineering Technical Conferences and Computers and Information in Engineering Conference*, 2016.

[5] F. Lamping, S. N. Gorb, and K. M. de Payrebrune, "Frictional properties of a novel artificial snakeskin for soft robotics," *Biotribology*, vol. 30, p. 100210, 2022.